Matti Autioniemi • Heikki Konttaniemi & Chris Händel

B

Detecting Passive Radar Reflectors for Automotive Applications

Aurora Arctic Challenge Field Tests in 2018

Co-financed by the European Union
Connecting Europe Facility

LAPLAND UAS PUBLICATIONS
Series B. Research reports and Compilations 7/2019

Detecting Passive Radar Reflectors for Automotive Applications

Matti Autioniemi, Heikki Konttaniemi & Chris Händel

Detecting Passive Radar Reflectors for Automotive Applications

Aurora Arctic Challenge Field Tests in 2018

Publication series B. Research reports and Compilations 7/2019

Lapland University of Applied Sciences
Rovaniemi 2019

ISBN 978-952-316-279-2 (pdf)
ISSN 2489-2637 (verkkojulkaisu)

Lapland University of Applied Sciences Publications
Series B. Research reports and Compilations 7/2019

Financiers: Aurora, Co Financed by the European Union - Connecting Europe Facility,
Traficom - Finnish Transport and Communications Agency, Väylä - Finnish Trasport Infrastucture Agency

Writers: Chris Händel (Roadscanners),
Matti Autioniemi & Heikki Konttaniemi
Covers &Layout: Lapland UAS, Communications

Lapland University of Applied Sciences
Jokiväylä 11 C
96300 Rovaniemi

Tel. + 358 020 798 6000
www.lapinamk.fi/julkaisut

Lapin korkeakoulukonserni
LUC

The Lapland University Consortium LUC is a strategic alliance between the University
of Lapland and Lapland University of Applied Sciences
www.luc.fi

Contents

List of Abbreviations

ACC	Adaptive Cruise Control
AEBS	Advanced Emergency Braking Systems
CAN	Controller Area Network
CW	continuous wave
FFT	fast Fourier transformation
FMCW	frequency modulated continuous wave
FoV	Field of view
FTA	Finnish Transport Agency
GPR	ground penetrating radar
IF	intermediate frequency
LiDAR	light detection and ranging
PLC	programmable logic controller
PLL	phase-locked loop
RCS	radar cross section
TI	Texas Instruments
TraFi	Transport Safety Agency

List of Figures

1. Introduction

Road transport is becoming increasingly automated with the new autonomous vehicles [1]. Some of the highly automated vehicles are still in the research and development phase, even though there are already automated cars driving on public roads [2]. In most of the cases, the high level of automation is greatly based on the ability of the vehicle to sense its surroundings by utilizing a set of sensors such as LiDARs (light detection and ranging), radars, GPS, ultrasonic sensors and cameras [3, 4].

Most of the automated vehicle tests are currently carried out in snow-free areas. However, there are numerous challenges that arise when testing autonomous functions in snowy and icy road conditions. Drifting and blowing snow practically blocks the vision of any camera system while causing major difficulties for LiDAR systems as well. On snow-covered roads the lane markings are not visible either. The availability of satellite positioning is more limited in Arctic areas and magnetic storms, i.e. the Aurora Borealis phenomenon, causes difficulties for GPS [5].

On the other hand, the presumption is that the current automotive radar systems could penetrate blowing or drifting snow and sense the surroundings in harsh winter environments. Consequently, with the help of strongly reflective roadside objects, automotive high-frequency radars could aid the navigation in snowy areas.

Passive roadside reflectors for automotive radars are one of the research topics in the Arctic Challenge research project. The project is divided into four main research questions that are all related to automated driving in snowy and icy conditions. This report focuses on the following research question: What landmarks, such as delineators and reflective posts, or snow poles and plot access marks, support automated driving? Where should these be located? What should they be like?

This test report is the second deliverable of the research that focuses on testing passive roadside radar reflectors. It is a continuation to the state-of-the-art review that was published in late spring 2018 in the publication series of research reports and compilations of the Lapland University of Applied Sciences Ltd. (Lapland UAS) [6]. This report describes the practical tests carried out in Rovaniemi, Finnish Lapland mainly during the winter period 2017-2018. The more detailed questions related to the research interests are the following:

1. How do different commercial passive radar corner reflectors compare in terms of reflective properties for an automotive application?
2. What is the effect of snow on the performance of a passive corner radar reflector?
3. What is the influence of typical roadside furniture on radar signals?

The report demonstrates some practical measurements and discusses them. It acts as input information for selecting the radar reflectors to be used on the Aurora intelligent test road in Finnish Lapland during 2018-2019 winter tests. Chapter 2 focuses on giving relevant background information on radar techniques and concepts as well as radar reflectors techniques. The actual test methods and equipment are described in more depth in Chapter 3, which is about the test area, tested radars and passive radar reflectors. Chapter 4 presents the measurements and discusses them from the point-of-view of the detailed research questions. Chapter 5 gives the reader an outlook of the report and concludes the report with some recommendations for the next steps in the research.

2. Background

2.1 RADAR TECHNIQUES

The abbreviation radar stands for radio detection and ranging and includes different detection systems based on radio waves (3 MHz – 110 GHz) [7]. Radio waves typically interact weakly with dust, fog, rain and falling snow, making them a suitable tool to perform measurements outdoors, under extreme weather conditions [8]. The advantages of radar are commonly used in traffic control, in meteorology (weather radar), in earth sciences (GPR) as well as in the automobile industry (ACC, parking assistant) [9].

2.1.1 The Working principle of Radar Systems

A typical radar setup includes a transmitter generating radar waves, e.g. via a magnetron or klystron [10]. The radar waves are guided to a transmitting antenna (TX) where they are emitted as primary signal in the space. The emitted primary signal is then reflected and scattered by a target depending on its conductivity $[\sigma] = (\Omega m)^{-1}$ [9, 11]. Targets with a lower conductivity reflect radar waves worse than ones with higher conductivity [11]:

$$E = \sigma J \tag{1}$$

$[E] = Vm^{-1}$ is the electric field and $[J] = Am^{-2}$ the current density. A receiving antenna (RX) detects the backscattered signal after a time Δt. If the transmitting and receiving antenna is the same device, a duplexer can switch the antenna between the transmitter and receiver. The receiver amplifies and demodulates the detected radio waves. The described working principle is illustrated in figure 1.

2.1.2 Radar Concepts

A common way to classify radar systems is based on the applied technology (see figure 2a). Radar systems, which measure only passive reflected signals from a target, are called primary radars. If the target is connected to an additional transponder, reacting to the primary signal and sending its own signal back to the receiver antenna, the system is called a secondary radar. [10]

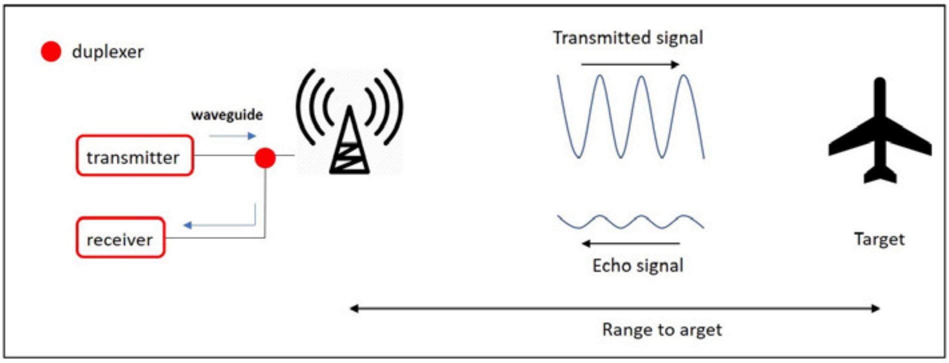

Figure 1 Principle setup of a radar system.
The setup contains a transmitter, an antenna, a duplexer and a receiver. Adapted from [7].

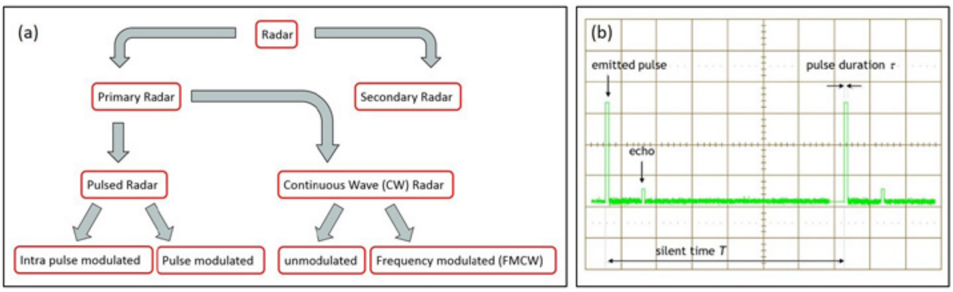

Figure 2 Classification of radar systems and the principle of pulsed radar.
(a) Classification of radar systems depending on the applied technologies. Adapted from [10]. (b) The working principle of pulsed radar. Adapted from [10].

As illustrated in figure 2a, primary radars can be classified as pulsed and continuous wave (CW) radars depending on their emitted signal form. The first mentioned systems emit µs-pules and receive the reflected signal after a time Δt. The silent period T between two pulses has to be large (ms-range) compared to the pulse duration (figure 2b). Assuming a linearly propagation of radio waves at a constant speed of light c, the distance R to the target can be calculated only from the runtime Δt of the emitted signal to the target and back [10]:

$$R = \frac{c \cdot \Delta t}{2}. \tag{2}$$

The direction of the target can be determined due to the angle dependency of the transmitted and reflected signal power (see figure 3a). Finally, the position of the target can be calculated using the measured parameters distance (length) and the direction (angle). [10]

In contrast to pulsed radars, CW radars send quasi-continuous signals. If the sent radar waves are unmodulated in frequency and amplitude, the relative velocity of the target Δv can be estimated via the Doppler shift between the sent and received signals [11]:

$$f = \left(1 + \frac{2 \cdot \Delta t}{c}\right) f_0. \tag{3}$$

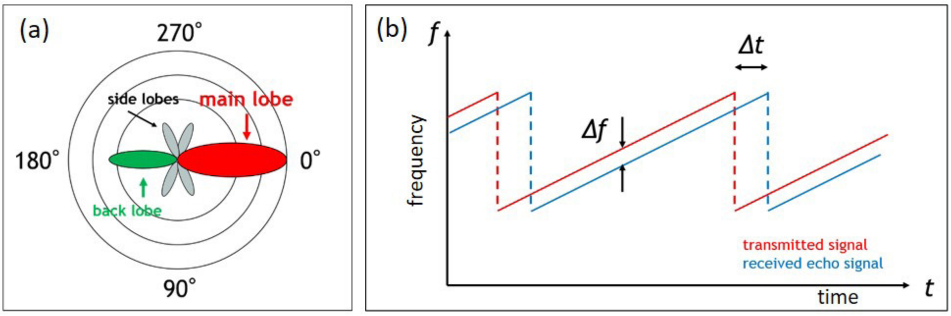

Figure 3 An antenna pattern and the general principle of FMCW Radar.
(a) Radiation pattern of an antenna in a polar-coordinate graph which faces to 0°. Adapted from [12, 13]. (b) The principle of FMCW Radar illustrated in a frequency-time plot. Adapted from [14]

f is the sent and f_0 is the received frequency. The distance between the target and the radar, however, remains unknown. CW radars with unmodulated signals are often applied for traffic speed controls. The distance between the target and the radar can be estimated by using periodically frequency modulated (FMCW) radar waves. A commonly used modulation pattern is the sawtooth (see figure 3b). The time Δt and the frequency shift Δf between the sent and received signal can then be used to calculate the target´s distance [10]:

$$R = \frac{c}{2}\Delta t = \frac{c}{2}\frac{\Delta t}{df/dt}. \tag{4}$$

The FMCW concept is often used in weather radars and in air traffic control. Considering the importance for automotive applications, the working principle of FMCW radars will be discussed in more detail in the next section.

2.1.3 FMCW Radars

As discussed in the previous section the emitted signal of FMCW radars is a linear chirp (signal with changing frequency) generated by a synthesizer. Each reflector in the area, illuminated by the radar, sends the emitted signal back. The received signal is then composed of multiple delayed and damped copies of the emitted chirp signal (figure 4a) corresponding to the different targets. Overlapping the reflected radar waves with the oscillator signal yields a beat-frequency (also intermediate frequency - IF) output. Applying a fast Fourier transformation (FFT) of the received IF signal produces a beat frequency spectrum, which is characterized by frequency peaks correlated with various objects. [15]

A Doppler component in the beat-frequency (phase shift of the beat signal from one chirp to another) is caused by the relative velocity between sender and reflector. This Doppler component can be accomplished by a second FFT over multiple chirps. Finally, the measurement includes a one-dimensional FFT of the received signals corresponding to each chirp (range-FFT) followed by a second two-dimensional FFT of this output over the chirps (Doppler-FFT).

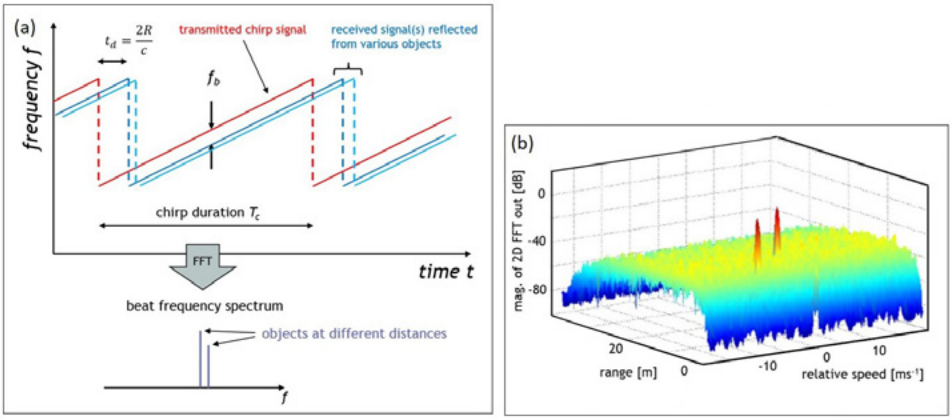

Figure 4 Working principle of FMCW and an output of the 2-D FFT procedure.
(a) Principle of FMCW radar and beat-frequency spectrum. [14] (b) Radar 2-D FFT image. [14]

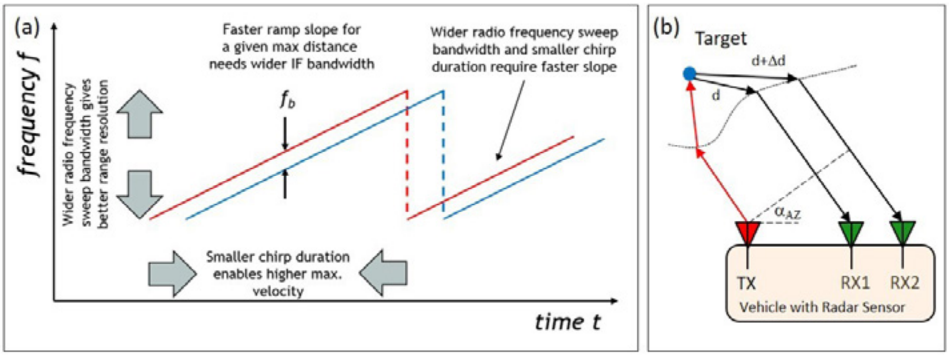

Figure 5 The influence of the chirp in the FMCW concept and the angle estimation.
(a) Dependency of range and speed from the chirp parameters. Highly linear chirps can be generated using a closed-loop phase-locked loop (PLL). [14] (b) The estimation of the angle is based on the observation that a change in the distance of a target results in a phase change in the peak of the FFT. At a minimum, two RX (receiving antennas) are required to estimate the angle of arrival via relative delays. Adapted from [15].

The second FFT enables the detection of several targets and a calculation of the targets range and velocity without ambiguity (see figure 4b). The dependency of range, velocity and angular resolution on the parameters of the chirp is summarized in figure 5a. The chirp parameters are crucial for a clear separation between multiple targets. [14]

An angle estimation for detected objects as well as 3D images (range, relative speed and angle) of the measured area can be performed using multiple antenna chains. Hereby, the angle is calculated by measuring relative delays of the received signal across multiple receiving antennas (see figure 5b). A larger number of antennas improve the angular resolution. [15]

2.2 REFLECTOR TECHNIQUES

Radar reflectors are designed to strongly reflect radar waves and can be applied to mark badly reflecting targets. Boats and bridge abutments are typical objects that are equipped with radar reflectors to ensure their detectability on radar systems. On smaller scales, reflective beads can be used in paints and foils [16] as well as on traffic signs or in automobile and bicycle tail lights [17]. A physical material property, describing the efficiency of reflectors, is the radar cross section (RCS) [7].

2.2.1 Radar Cross-Section

The RCS is the area of a hypothetical isotropic reflective surface, which would produce the same strength echo signal as the reflector itself. A sphere with an ideal conducting surface (1 m² projection surface) is used as reference (see figure 6a). For example, a radar reflector with a RCS of 15 m² has the same effective reflective surface as 15 of these ideal reference spheres. Typical RCS values are given in figure 6b. [7]

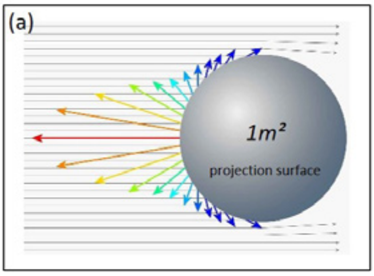

(b)	Radar cross-section [σ] = m²
Small bird	0.01
Human body	1
Luneburg lenses	5-250
Large commercial airplane	100
Corner reflector (a = 1.5m)	20379

Figure 6 Radar cross section.
(a) Illustration of the hypothetical ideal conducting sphere used as a reference system. Only a small part of the surface acts in retro-reflection (red, orange). The other part of the sphere distributes the radar waves back to the emitter. [18] (b) Values of the radar cross-section from selected objects. The values are for a wave in cm-range. [7, 19–21]

Beside the material, the RCS of a reflector depends also on its geometry as well as on the properties of the incoming radiation (wavelength, polarization and angle). The RCS can be generally defined as:

$$\sigma = 4\pi R^2 \frac{P_{scat}}{P_{em}}. \quad (5)$$

$[P_{scat}] = Wm^{-2}$ is the scattered power density at a distance R from the reflector and P_{em} is the power density of the radiation at the reflector. [7]

2.2.2 Radar Reflectors

The working principle of radar reflectors is often based on retro-reflection. Retro-reflection means reflection of receiving radiation independently from the orientation of the reflector. Retro-reflection can be realized via corner reflectors, spherical reflectors or phase-conjugated mirrors. The following discussion will mainly be restricted to the first mentioned, because of their central role for radar applications. [22]

Metallic corner reflectors have an excellent reflecting behavior for radar waves while corner reflectors made of glass prisms are often used for LiDAR systems. Common corner reflectors consist of three mutually perpendicular, plane and conductive surfaces, which reflect the electromagnetic wave up to three times (figure 7a). The reflection on several perpendicular planes is phase synchronous, due to the equal lengths of the single phases (figure 7b). [22]

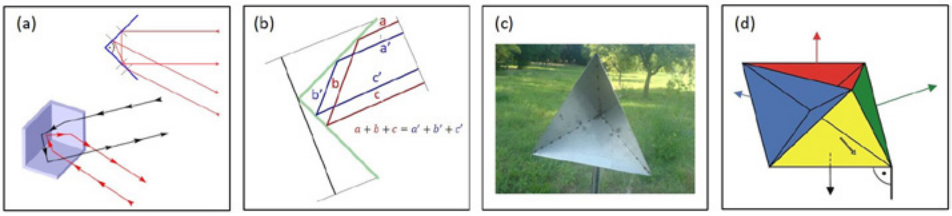

Figure 7 Corner reflectors.
(a) The working principle of a corner reflector. The radar wave is reflected back along a parallel vector to the radar source. [22, 23] (b) An illustration of an “in phase reflection” due to equal lengths a+b+c = a'+b'+c'. [24] (c) A triangular corner reflector for radar testing. The metal surfaces are attached to each other at the edges forming a corner. [22] (d) An arrangement of corner reflectors in an octahedron shape. [25]

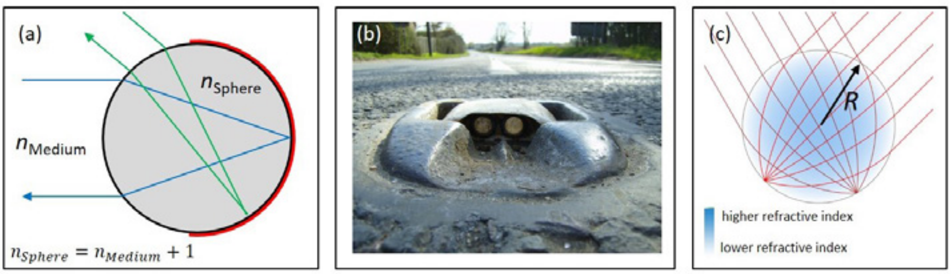

Figure 8 Spherical retroreflectors.
(a) A sketch of a spherical reflector (with two light rays in blue and green) consisting of a refractive transparent sphere (gray) combined with a reflective surface (red). Adapted from [22] (b) Cat’s eye pavement marker. [22] (c) Optical path in a Luneburg lens. The gradient in the refractive index n is sketched in blue and increases from the surface to the centre. [26]

The RCS can be estimated for triangular (figure 7c) and cubic corner reflectors with [27, 28]:

$$\sigma_{tr} = \frac{4\pi a^4}{3\lambda^2} \qquad \sigma_{cub} = \frac{12\pi a^4}{\lambda^2}. \tag{6}$$

a is the edge length of the isosceles triangle and λ the wavelength of the radar radiation. The surfaces of the reflector should be large compared to the used wavelength ($\lambda \ll a$). If the setup requires reflectivity in all directions, eight triangular corner reflectors can be combined (figure 7d).
Retro-reflection can further be realized with lens-like systems such as spherical reflectors (figure 8a). Cat’s eye pavement markers (figure 8b) and strongly reflective paints are only two examples of this reflector type. A typical spherical retro-reflector is composed of a refractive transparent sphere whose focal surface corresponds with a reflective surface like a spherical mirror [22]. Optical inaccuracies, caused by aber-

rations, can be solved with the Luneburg lens concept. Luneburg lenses work with a spherically symmetrical index gradient [29]. The gradient is built in such a way that parallel incoming waves are focused on the same point (figure 8c) [29]. An introduction to both physical concepts is given in [22, 30].

3. Materials and Methods

3.1 TEST FIELD, OUTER CONDITIONS AND TEST PREPARATION

To guarantee comparable conditions between different experiments, the tests were performed on a test track from Lapland UAS near the airport of Rovaniemi (figure 9a). The test field is 165 m long and 25 m wide (southern part only). Further, the experiments were performed under arctic conditions ($\theta \approx$ -15 °C, ≥ 1 m snow, rough ground, slope), (figure 9b). The radar enclosure height was 60 cm over the ground (figure 9c).

3.2 APPLIED RADAR SYSTEMS

Radars have become increasingly important for automotive applications in the last decade. The systems can operate in almost all environmental conditions making them indispensable for technologies supporting autonomous driving, such as advanced emergency braking systems (AEBS) or adaptive cruise control (ACC). Particularly, the frequency range between 76 and 81 GHz (≈3 mm) has been established in this field, which facilitates small and compact antenna geometry. The wide bandwidth available further enables high accuracy and object resolution. [14]

In the following sections, three selected radar systems will be introduced. The systems from Continental AG, Furuno Electric Co., Ltd. and Texas Instruments Inc. (TI) are suitable for transport applications and formed the basis of the measurements described in section 4.

3.2.1 ARS 408-21 from Continental AG

The 408-21 Premium sensor from Continental (figure 10a) is a robust and small radar sensor operating with a frequency of 77 GHz. The sensor is designed for automotive applications and works with a dual scan (serially alternating). The dual scan principle enables switching between far- and short-range detection (figure 10b). The switching between the two ranges is realized via different chirps. The system further includes multiple antennas for simultaneous detection of objects. A classification of moving objects as vehicles or pedestrians, based on the RCS or the objects velocity, is also possible. In order to minimize the influence of moisture and other environmental disturbances to the radar, the sensor was enclosed with a plastic box (figure 10c). The system was further equipped with a metallic holder to fix it in front of a vehicle for future mobile measurements.

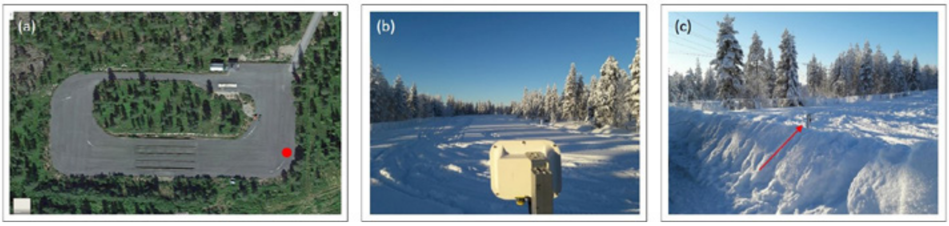

Figure 9 Test field in Rovaniemi.
(a) Aerial photograph of the test track (66°32'52"N 25°48'36"E) [31]. The red dot shows the position of the radars. (b) Test track in January 2018 before a measurement. (c) Position of the radar in the test field.

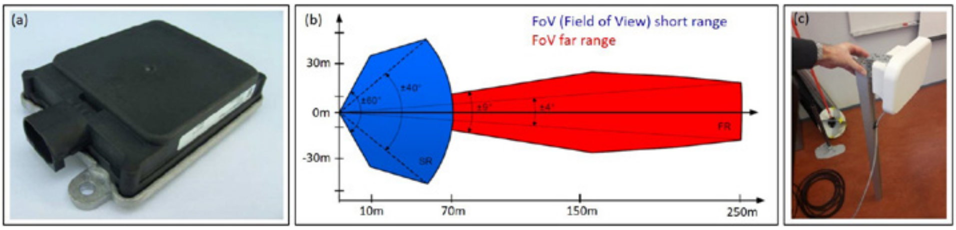

Figure 10 ARS 408-21 radar sensor.
(a) Picture of the ARS 408-21 radar sensor. [32] (b) A digital antenna offers two independent scans for far and short range. The sensor contains 2 TX and 6 RX antennas for near range and 2 TX and 6 RX antennas for far range scan using digital formed beams. [32] (c) Self-designed enclosure.

Prior to a measurement, the radar sensor was connected to a CAN (Controller Area Network) module performing the communication between the computer and the radar.

The radar's working principle is based on fast chirp FMCW modulations performing an independent distance and velocity monitoring of targets in one cycle (see section 2.1.3). The target information is evaluated during every cycle and its position is given in a coordinate system relative to the sensor. The target's speed is calculated relative to an assumed vehicle trajectory, which is estimated by using the velocity and yaw rate information (if the radar is fixed in the longitudinal direction on the front of the vehicle). The detected targets can be filtered by different criteria (e.g. RCS) and thus only reflections of objects of interest are sent to the CAN-bus. A technical description of the radar is provided in [33]. A Radar PLC (Programmable logic controller) was used to display the measured data on a monitor.

3.2.2 DRS4D-NXT from Furuno

The second radar, which was chosen for the experiments is the DRS4D-NXT from Furuno (figure 11a). This 9.4 GHz solid-state pulse compression Doppler radar has been developed for maritime applications and can simultaneously detect up to 100 objects. Additionally, the radar was equipped with a metal mount to enable mobile measurements on top of a vehicle (figure 11b). The radar further includes a target analyzer; a fast target tracking and auto target acquisition function to offer optimal detection of hazardous objects. Targets moving towards the radar automatically change the color to support the identification of targets. Data monitoring was carried out with the NavNet TZtouch2 display (figure 11c). An included rain mode enabled target detection even during hard weather conditions. A technical description can be found in [34].

Figure 11 DRS4D-NXT radar sensor from Furuno.
(a) Picture of the enclosure of the DRS4D-DRS4D-NXT radar sensor [34]. (b) DRS4D-DRS4D-NXT radar sensor mounted on top of a car for mobile measurements. (c) Picture of the NavNet TZtouch2 display. [35]

3.2.3 AWR1642BOOST from Texas Instruments

The AWR1642 device is an integrated single-chip FMCW radar sensor capable of operation in the 76- to 81-GHz band. It is an ideal solution for low power, self-monitored, ultra-accurate radar systems in the automotive space (figure 12a). The radar includes four receiving and two transmitting antennas and can operate in the ultra-short range as well as in longer distances (figure 12b). Further specifications of the sensor are given in [36].

An evaluation module named AWR1642BOOST is available for the described AWR1642 radar (figure 12c). The evaluation module was equipped with a mmWave-DEVPACK to configure the system with the “Radar Studio” software. The software enables visualizing and post-processing of the measured data. The module was further equipped with a “TSW1400 EVM” high-speed data capture/pattern generator to get raw analog data from the radar. Finally, the radar system was protected with a self-designed enclosure (figure 12d). [37]

3.3 APPLIED RADAR REFLECTORS

Autonomous driving could become the most important transformation in automobile industry in the current century [38]. Hereby, an accurate and reliable detection of vessels and other objects such as physical land infrastructure is a challenging task for scientists and engineers. Passive radar reflectors could be the key to overcome detections problems under extreme weather conditions, such as falling rain and snow. In the section 3.3.1, four passive radar reflectors in different form and size will be described. All of them were commercially used in the maritime sector. In contrast to commercially used radar reflectors, four self-designed corner reflectors will be introduced and discussed in section 3.3.2.

3.3.1 Commercially Used Radar Reflectors

Corner reflectors, commercially used in the maritime sector, are often composed of anodized aluminium. They are widely octahedral shaped or stacked dihedrals in a vertical plane. Octahedral reflectors are typically diamond-shaped or constructed from circular panels slotted together. [39]

For the following experiments, four radar reflectors were chosen and acquired. The models are presented in figure 13. First, an octahedral, circular 40 cm reflector consisting of anodized aluminium circular panels.

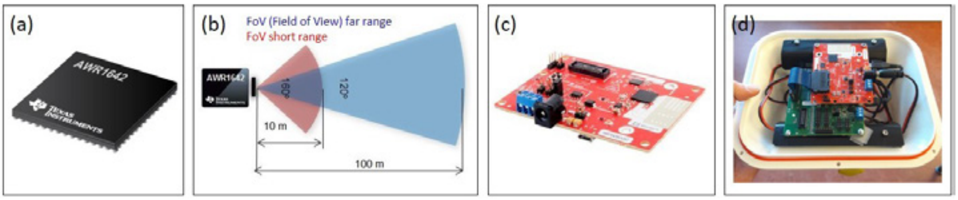

Figure 12 AWR mmWave front-end sensors.
(a) Picture of the AWR1642 76-to-81 GHz high-performance automotive radar sensor. [36] (b) AWR1642 single chip sensor and its range, field of view (FoV) capability. [40] (c) Picture of the AWR1642BOOST - AWR1642 76-to-81 GHz high-performance automotive radar sensor evaluation board. [37] (d) Self-designed enclosure to protect the radar from moisture and other disturbances.

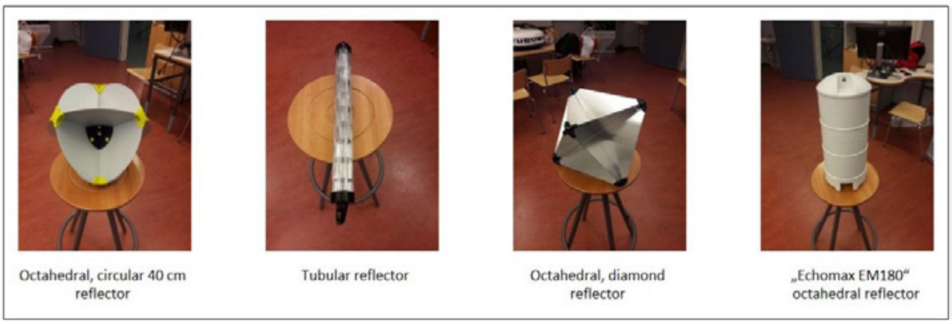

Figure 13 Radar reflectors used in the maritime sector.
Shown is a selection of four commercially used common radar reflectors.

The second model is a tubular reflector. The reflector consists of an array of dihedrals (stacked in the vertical plane), which are encompassed within a clear plastic body. An octahedral reflector, composed of three aluminium diamonds, which are slotted together, was the third chosen model. The panels are locked in placed by plastic corner pieces. This reflector only had mounting holes for an upright position. Finally, the Echomax EM180 comprises a vertical stack of three aluminium corner arrays enclosed in a plastic case. It relies upon interactions between each of the arrays to produce large peak responses. A performance investigation of the reflectors has been carried out for meeting the standards of maritime transport. The results and conclusions are presented in [41].

3.3.2 Self-designed Corner Reflectors

To test also more practicable, cheaper and easy to produce corner reflectors, Lapland UAS designed and acquired four versions of self-designed octahedral corner reflectors. The principle (figure 14a) of the self-designed reflectors is similar to the commercially used octahedral, circular 40 cm reflector described in the last section. Self-designed were small (Ø 1.649 cm), medium (Ø 4.05 cm), large (Ø 10 cm) and extra-large (Ø 20 cm) prototypes made from aluminium (10 respectively, figure 14b and d). For preliminarily tests, the reflectors were fixed on top of plastic poles (figure 14c).

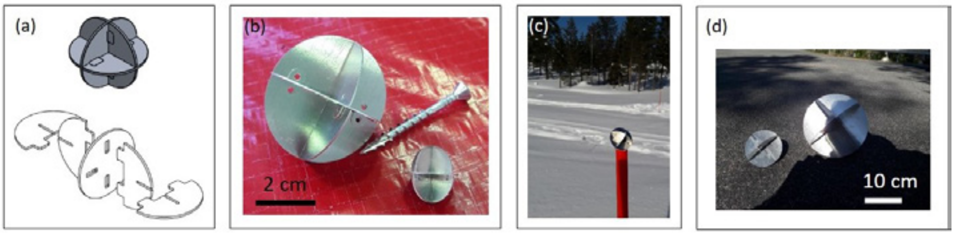

Figure 14 Self-designed aluminium reflectors.
(a) Sketch and design drawing of the self-designed corner reflectors. (b) Medium (left) and small (right) self-designed corner reflector. Shown is one prototype respectively. (c) Self-designed corner reflector (medium version) on top of a plastic pole (60 cm high). (d) Large (left) and extra-large (right) self-designed corner reflector. Shown is one prototype respectively.

4. Results and Discussion

In the following sections, the experimental results from different radar and reflector tests are presented and discussed. The tests were prepared and performed as described in section 3.1. First, in section 4.1, the test field only was monitored by different radar systems to identify strong reflecting background objects. In section 4.2 the influence of human presence on the radar signal was studied to estimate its effect on further results. In section 4.3 four different radar reflectors from the maritime sector were tested regarding their detectability, reflectivity (RCS) and practicability for our applications. Further, four self-designed reflectors were tested. Based on the previous results, a mobile test was carried out. Its results are presented in section 4.4. Finally, the effect of snow and roadside furniture on the radar signal was studied in sections 4.5 and 4.6.

4.1 THE TEST FIELD BACKGROUND

In order to obtain comparable starting conditions, a reference measurement was performed with each radar system. In these experiments the test field only was monitored as a background. Equipment or humans were not present on the test track during the measurement. The characterization of typical objects in the surroundings and their RSC was a further goal of this measurement.

Figure 15a demonstrates the empty rectangular test field monitored with the ARS 408-21 from Continental. The plot shows only reflections with RCS of 16 m^2 or more. Weaker reflections were filtered out. The surroundings of the test field are characterized by multiple strong reflections. These reflections are caused among others by big trees and wires at the upper end of the test track (figure 15b). The test field itself is free of reflections. Figure 15b shows the two different views (near and far field) introduced in section 3.2.1. The dashed rectangle in the center of the plot shows the "view of interest" used for most of the test cases discussed later. This "view of interest" is separately shown in figure 15c including some strong and stable reflections. The reflections are caused by stationary poles and a metal fence on the side. The duration of the data collection was 61 s. The radar stored 136 data points per identified object in 10 s.

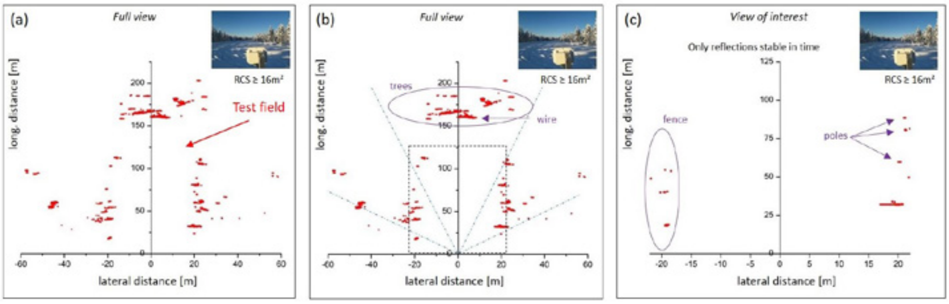

Figure 15 Test field background measured with the ARS 408-21 from Continental. (a) Longitudinal - lateral distance plot of the rectangular test field (overview). Shown are only reflections (red) with a RCS of 16 m² or higher. (b) Illustration of two different fie ld of views (near and far field). The strong reflections in the background are caused be wires and multiple big trees. (c) View of interest with a max. longitudinal distance of 125 m. Clearly visible are stationary metal poles on the right side as well as a metal fence on the left side. This view was mainly used for the measurements with radar reflectors.

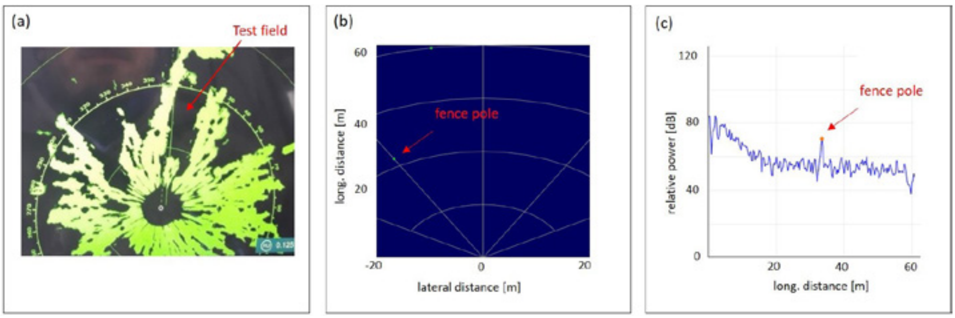

Figure 16 Test field background measured with the sensor from Furuno and Texas Instruments. (a) Screenshot of the NavNet TZtouch2 display (from Furuno) during the measurement. Shown is the longitudinal - lateral distance view of the rectangular test field and the surrounding area. (b) Longitudinal - lateral distance plot of the test field recorded with the radar from TI. (c) Range profile measured with TI radar. The orange dot shows the detected object.

The test field was further monitored with the DRS4D-NXT from Furuno. Similar to the results obtained from the Continental radar, the test track is clearly visible and occurs free of radar reflections, while the surroundings are characterized by numerous strong reflecting objects (figure 16a). Single objects, such as wires or fence poles, could not be resolved with the radar from Furuno. Raw data storage and processing (e.g. RCS) was, in contrast to the Continental system, not possible. The signal strength of different areas could roughly be compared using a colour scale, whereas absolute RCS values were not recorded by the radar.

Figure 16b shows the empty test field as a longitudinal – lateral distance plot monitored with the AWR1642BOOST from TI. The maximum longitudinal distance is limited to 60 m (due to the BOOST demo version). One fence pole on the left side was detected as a strongly reflecting object. A signal strength – longitudinal distance plot (figure 16c) enables the estimation of signal strengths. The duration of the data collection was 10 s. The radar stored 100 data points per object in 10 s.

4.2 THE INFLUENCE OF HUMAN PRESENCE

In the following experiments a human, dressed in conventional winter clothes, stood and walked in the test field. Additional reflectors were not present in the track during the measurement.

First, the human stood unmoving, 100 m (in longitudinal direction) away from the radar, in the test field. The test field was monitored for 64 s with radar from Continental. The experiment was repeated at 30 m (40 s). At both longitudinal distances the human could not be detected by the radar (figure 17a). Under the same experimental conditions, the human walked in a third test from a position 50 m away from the radar towards the radar (figure 17b). The human was again not detectable with the chosen noise level (RCS ≥ 16 m²).

The experiments were repeated with the radars from Furuno and TI. The 100 m distance was excluded for the TI radar, due to the restricted maximum range. A standing or walking human was not detectable with the radar from Furuno nor with the TI radar. Representative results are illustrated in figure 17c and figure 17d.

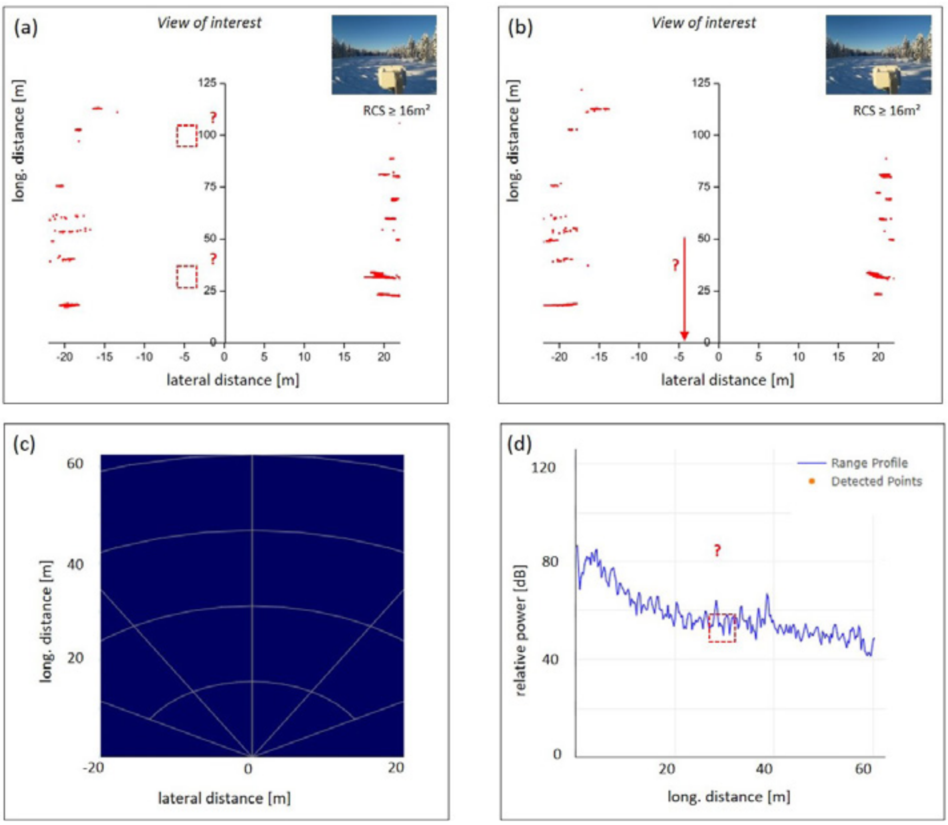

Figure 17 Reference measurements with a human in the test track.
(a) Longitudinal-lateral distance plot measured with the Continental radar. The human stood at two different positions (red boxes) unmoving during the measurement. (b) Longitudinal-lateral distance plot measured with the Continental radar. The human walked from a position 50 m away from the radar to the radar (red arrow). (c) Longitudinal-lateral distance plot measured with the TI radar. The human stood unmoving 30 m in front of the radar. (d) Range profile measured with TI radar.

4.3 RADAR AND REFLECTOR TESTS

In the following sections the experimental results from the radar measurements of different radar reflectors are presented and discussed. In section 4.3.1 the octahedral, circular 40 cm reflector is tested with the three radar systems on different longitudinal positions. The experiments will show the strengths and disadvantages of the applied radars concerning our future applications. Further, an experiment in which the reflector was shifted is discussed in section 4.3.2. The experiment should determine whether a strong reflecting object can be detected constantly while it is moving. It should further give an impression of the angle dependency of the RCS. In addition to the octahedral, circular 40 cm reflector, three more reflectors from the maritime sector are studied regarding their detectability and reflectivity (RCS) in section 4.3.3. The tests shown in section 4.3.4 and 4.3.5 comprise four different self-designed reflectors along with a "road-like" test case. Both should act as a preparation for further mobile tests involving a driving vehicle.

4.3.1 The Octahedral, Circular 40 cm Reflector Monitored with Three Radar Systems

The octahedral, circular 40 cm reflector was tested on different longitudinal positions in the test field. Prior testing the reflector was fixed on a plastic pole and stuck in the snow on the chosen position. The reflector was always ≈60 cm above the ground (figure 18a).

At the beginning, the reflector was positioned 10 m in longitudinal and 5 m in lateral direction away from the radar. After accurate positioning, the test field was monitored for 60 s with radar from Continental and 50 s with the radar from TI. The experiment was repeated in 10 m-steps (longitudinal) while the lateral position was held constant. Each position was monitored in a separate experiment. Positions with larger longitudinal distances than 60 m were excluded for the TI system.

Figure 18b demonstrates the echoes measured with the radar from Continental. The echoes are clearly visible as isolated points in the plot. The corresponding RCS values are given in figure 18c. The values range from σ (80 m) = (18±3) m^2 to σ (60 m) = (794±113) m^2. This deviation is based on the angle dependency of the RCS. The time-dependence of the RCS during the observation is shown for two selected representative longitudinal distances in figure 19. The RCS of the reflector is higher than the RCS of background objects in the test field. The detected accuracy is ±0.1 m in longitudinal and ±0.2 m in lateral directions.

The reflector could also be detected with the radar from TI. Figure 20a-c shows the reflector on three representative longitudinal distances and the echoes are displayed as isolated points. The signal produced by the reflector is clearly over the noise level as the corresponding range profiles below the longitudinal-lateral distance plots show.

The test was further performed with the DRS4D-NXT system from Furuno. Similar to the results obtained from the Continental and TI radar, the reflector is detectable but occurs as diffuse spot in the test field. Figure 20d shows the reflector on two longitudinal positions. Due to the range resolution of 20 m, the range accuracy of 10 m (+ 1 % of the range in use) and the minimum range of 20 m, it was decided to restrict the experiments to 20 m intervals.

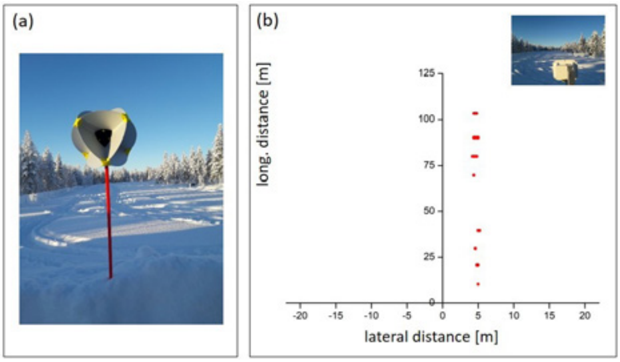

(c)

Longitudinal distance	Median RCS [m²]
100 m	79 ± 21
90 m	25 ± 15
80 m	18 ± 3
70 m	282 ± 20
60 m	794 ± 113
50 m	398 ± 40
40 m	22 ± 6,5
30 m	447 ± 56
20 m	44,5 ± 13
10 m	40 ± 3

Figure 18 The octahedral, circular 40 cm reflector tested with the sensor from Continental. (a) The reflector on a 60 cm high plastic pole while testing. (b) Longitudinal-lateral distance plot measured with the Continental radar. The red dots show selected reflections caused by the reflector. Each reflection was measured in a separate experiment. (c) RCS values measured with the radar from Continental on different longitudinal positions.

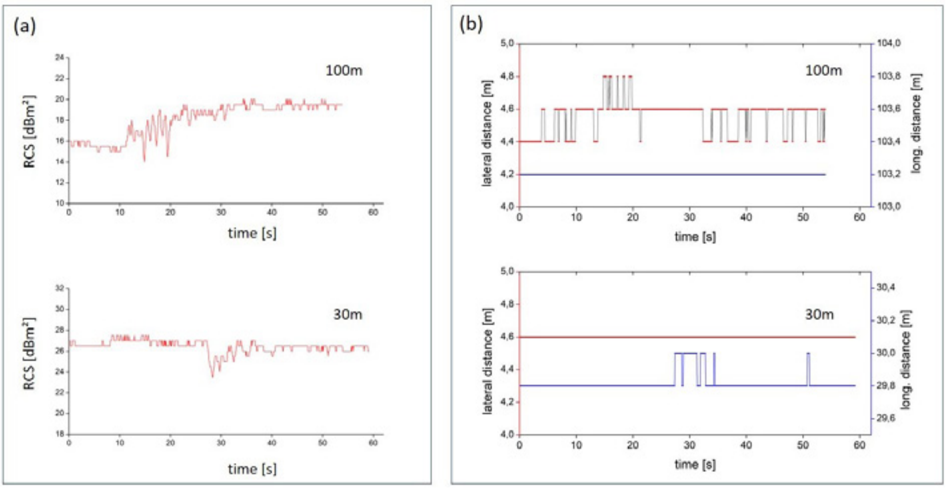

Figure 19 Time evolution of the echo signal recorded with the sensor from Continental. (a) RCS-time plot. The data was produced by the octahedral, circular 40 cm reflector. The reflector was positioned 100 m (top) and 30 m (bottom) in longitudinal and 5 m (both) in lateral direction away from the radar. (b) Time evolution of the lateral (red) and longitudinal (blue) distance for the same experiments as shown in (a).

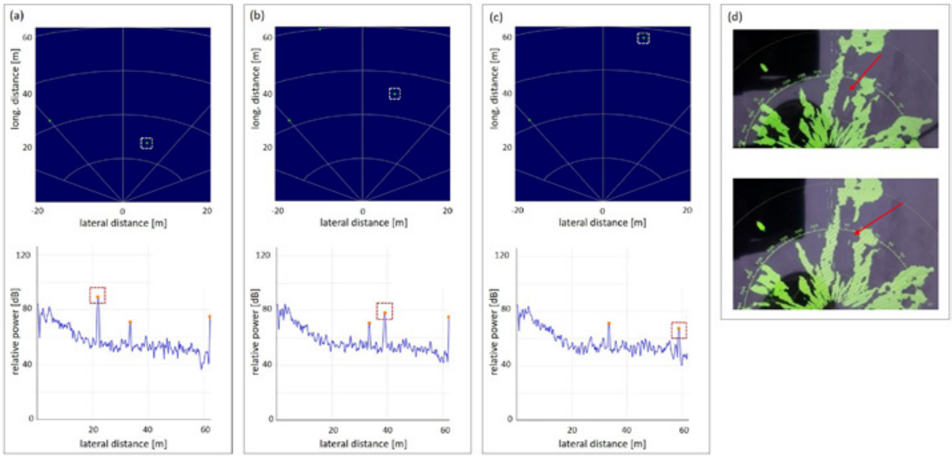

Figure 20 The octahedral, circular 40 cm reflector tested with the sensor from TI and Furuno. Longitudinal-lateral distance plots measured with the TI radar (upper blue graphs). The white rectangles show reflections caused by the reflector. Shown are 3 selected longitudinal distances: (a) 20 m, (b) 40 m and (c) 60 m. Each reflection was measured in a separate experiment. Below the longitudinal-lateral distance plots are the corresponding range profiles. The peaks caused by the reflector are marked in red. (d) Longitudinal-lateral distance plots measured with the Furuno radar. The red arrows show reflections caused by the reflector. Shown are 2 selected longitudinal distances: (a) 80 m, (b) 100 m. Each reflection was measured in a separate experiment.

4.3.2 The Octahedral, Circular 40 cm Reflector Shifted Towards the Radar

In addition to the tests based on reflectors at fixed positions (section 4.3.1), an experiment was performed in which the octahedral, circular 40 cm reflector was shifted from a longitudinal position 100 m away from the radar towards the radar. The experiment should determine if a strong reflecting object can be detected constantly with the selected radars while it is moving. The experiment should further give an impression of the angle dependency of the RCS.

To begin, the reflector was positioned 100 m in longitudinal and ±0 m in lateral direction away from the radar. After accurate positioning, the reflector was carried by a human towards the radar to the target position. The target position is 0 m in longitudinal and -5 m in lateral direction from the radar. While shifting ($\Delta t \approx 100$ s), the test field was monitored with radar from Continental. Due to the results shown in section 4.2 we expect no significant disturbance of the backscattered signal caused by the human presence. Further, the reflector was fixed on a plastic pole, which guaranteed a distance between reflector and human of at least 80 cm.

Figure 21a shows the echoes measured with the radar from Continental while the reflector was shifted. Figure 21a and 21b demonstrate that, the reflector is almost always detectable while it was shifted. During the shift, the angle between the radar and the reflector naturally changed due to the shifting path. Figure 21c clearly shows the strong angle dependency of the RCS (signal strength). The RCS values vary during the 100 s long shift between slightly over zero and 400 m². The result is in accordance with theoretical expectations introduced in section 2.2.1.

The experiment was further performed with the radars from TI and Furuno. In both experiments the reflectors were quasi constantly detectable.

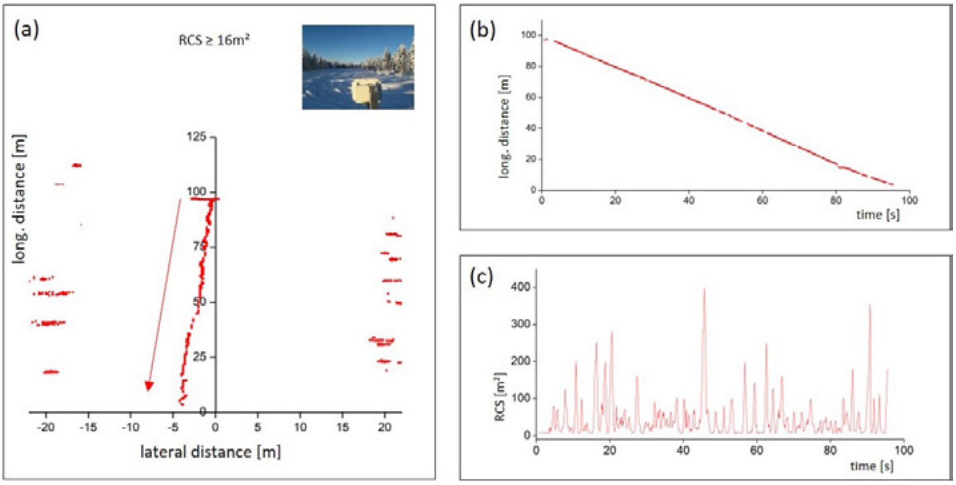

Figure 21 Shifted octahedral, circular 40 cm reflector measured with the Continental radar. (a) Longitudinal-lateral distance plot. The reflector was shifted from a position 100 m away from the radar towards the radar (red line in the centre). The red arrow shows the direction of movement. (b) Longitudinal distance-time plot for the shifted reflector. (c) RCS-time plot for the shifted reflector.

4.3.3 Other Reflectors from the Maritime Sector

In the following experiments a tubular reflector from Lalizas, the Echomax EM180 and another octahedral shaped reflector are studied regarding their detectability with different radars. Similar to the tests described in section 4.3.1 the reflectors were either fixed on a plastic pole or hung on a rope as shown in figure 22a. Both, the reflector and holder were positioned in such a way, that the reflector was always ≈60 cm above the ground.

Prior an experiment, the chosen reflector was positioned 20 m in longitudinal and 5 m in lateral direction away from the radar. After accurate positioning, the test field was monitored for 60 s with radar from Continental and 50 s with the radar from TI. The experiment was repeated in 20 m-steps (longitudinal) while the lateral position was held constant. Each position and each reflector was monitored in a separate experiment. Positions with larger longitudinal distances than 60 m were excluded for the TI system.

Figure 22b presents RCS values measured with the radar from Continental. The table further shows, that the tubular reflector is not detectable at all with ARS 408-21 sensor from Continental. The other two tested reflectors performed in a similar quality as the octahedral, circular 40 cm reflector shown in section 4.3.1. This deviation between the single values is based on the angle dependency of the RCS. The higher errors at 20 and 100 m are caused by a slight rotation of the reflector during the measurement.

Figure 23a-c shows the longitudinal-lateral distance plots and range profiles for the three reflectors respectively. The plots were produced with the radar from TI. All three tested reflectors are detectable with the radar from Texas Instruments even the tubular reflector which was not measurable with the Continental radar. The signal peak produced by the tubular reflector was weaker compared to the peaks from the other two reflectors.

The experiment was further performed with the radar from Furuno. All three tested reflectors are also detectable with the radar from Furuno. The tested reflectors occur as diffuse spot in the test field. The smallest spot was produced by the tubular reflector. The results are summarized in figure 23d.

(a)

(b)

Longitudinal distance	Tubular reflector	Octahedral d.	Echomax EM180
20m	not detectable	26 ± 25 m² *	56 ± 28 m²
40m	not detectable	126 ± 1 m²	28 ± 2 m²
80m	not detectable	200 ± 16 m²	126 ± 1 m²
100m	not detectable	71 ± 61 m² *	116 ± 60 m²

Figure 22 Behaviour of different radar reflectors measured with the system from Continental. (a) The reflector Echomax EM180 on a rope 60 cm above the ground. (b) Median RCS values measured in four different distances with the Continental radar. (* mean values)

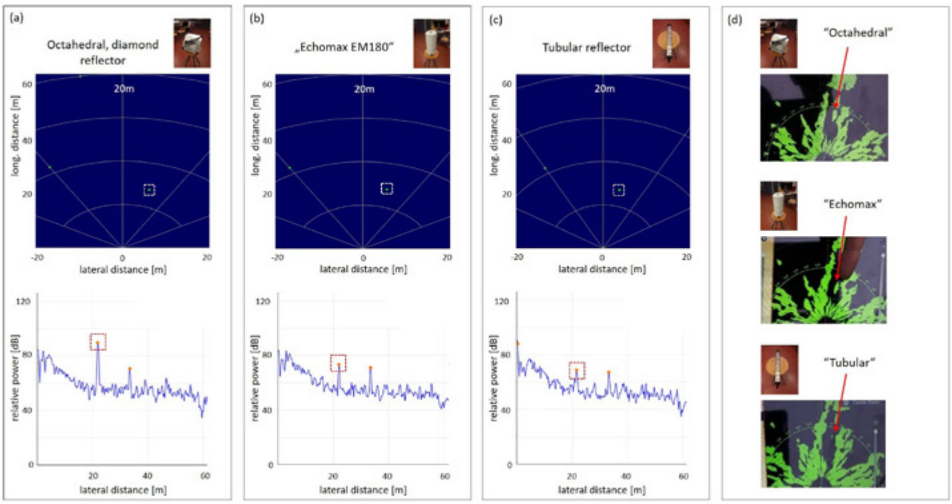

Figure 23 Behaviour of different radar reflectors measured with the radars from TI and Furuno. (a-c) Longitudinal-lateral distance plots measured with the TI radar (upper blue graphs). The white rectangles show reflections caused by the reflector. Presented are tests with a selected longitudinal distance of 20 m. Each reflection was measured in a separate experiment. Below the longitudinal-lateral distance plots are the corresponding range profiles. The peaks caused by the reflector are marked in red. (d) Longitudinal-lateral distance plots measured with the Furuno radar. The red arrows show reflections caused by the reflectors. Shown are experiments with a longitudinal distance between radar and reflector of 80 m. Each reflection was measured in a separate experiment.

4.3.4 Self-designed Reflectors

In order to study more practicable, cheaper and easy to produce corner reflectors, Lapland UAS designed, acquired and assembled four versions of self-designed octahedral corner reflectors (see section 3.3.2).

Prior testing the reflectors were fixed on a plastic pole 60 cm above the ground. The reflector was positioned 20 m in longitudinal and 3 m in lateral direction away from the radar. After positioning, the test field was monitored for 60 s with radar from Continental. The experiment was repeated in 20 m-steps (longitudinal) while the lateral position was held constant. The test with the longitudinal distance of 60 m was additionally measured on a lateral distance of -5 m due to a disturbance caused by concrete elements in the test field. Each position and each reflector was monitored in a separate experiment.

Figure 24a and b demonstrate the echoes produced by the two larger (Ø 10 cm and Ø 20 cm) self-designed reflectors. The echoes are clearly visible in the plot as isolated points. The corresponding mean and median RCS values are given in figure 24c. The RCS values of the Ø20 cm reflector are comparable to those measured for the octahedral, circular 40 cm reflector. Further, they are significantly higher compared to those RCS values detected for the Ø10 cm reflectors. The latter mentioned result is in accordance with the dependency between RCS and edge length of a reflector (section 2.2.2). The smaller differences between the values measured for the octahedral, circular

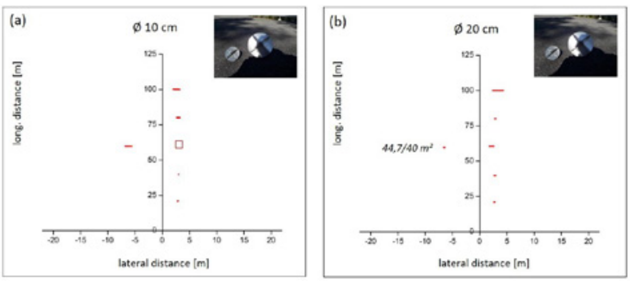

(c)

Longitudinal distance	Median/Mean RCS [m²] 10 cm	Median/Mean RCS [m²] 20 cm
100m	112/ 106	16/ 20
80m	9/ 9	200/ 186
60m	8/ 8	251/ 233
40m	9/ 9	79/ 169
20m	14/ 13	40/ 41

Figure 24 Self-designed reflectors tested with the 408-21 Sensor from Continental.
(a) Longitudinal-lateral distance plots for the Ø10 cm reflector. (b) Longitudinal-lateral distance plots for the Ø20 cm reflector. The red dots show the measured reflections caused by the reflector. Each reflection was measured in a separate test. The test with a longitudinal distance of 60 m was additionally measured on a lateral distance of -5 m. (c) Median and mean RCS values measured in five different distances.

40 cm reflector and the Ø20 cm self-designed reflector may result from the different designs. The two smaller (Ø 1.7 cm and Ø 4 cm) self-designed reflectors could not be detected (at all tested positions and angles) with the radar from Continental nor with the radar from Texas instruments.

The self-designed reflectors were not measured with the radar from Furuno due to the lower resolution of the device compared to the radars from Continental and Texas instruments, as well as the test results gotten in the previous sections.

4.3.5 A road-like case

In this section the test results from a road-like case are presented. The tests should act as preparation for further tests with a driving vehicle. As shown in figure 25a, the experimental setup consisted of 10 equal, self-designed reflectors (five on the left and five on the right side). The distance between the single reflectors was 20 m in longitudinal direction and 9 m (pairwise) in lateral direction. The radars position was chosen in a way that a vehicle on the road would have. Figure 25b shows the experimental conditions in the field while testing.

After positioning, the test field was monitored for 55 s with radar from Continental. All ten equally designed reflectors were simultaneously measured in one experiment. The experiment was conducted for the Ø 1.649 cm, Ø 4.05 cm, Ø 10 cm and Ø 20 cm self-designed reflectors, respectively. The two smaller reflector types could not be detected at all (figure 25c and figure 25d). In contrast to that result, the Ø 10 cm and Ø 20 cm reflectors could be detected with the Continental radar (figure 25e and figure 25f). The reflections are visible in the plots as isolated points. The corresponding mean and median RCS values are given in tables alongside.

Even though the RCS depends also on angle between the radar and the reflector, the RCS values measured for the Ø 20 cm self-designed reflectors are significantly higher compared to those for the Ø 10 cm reflectors. The test results are in accordance with the results presented in section 4.3.4.

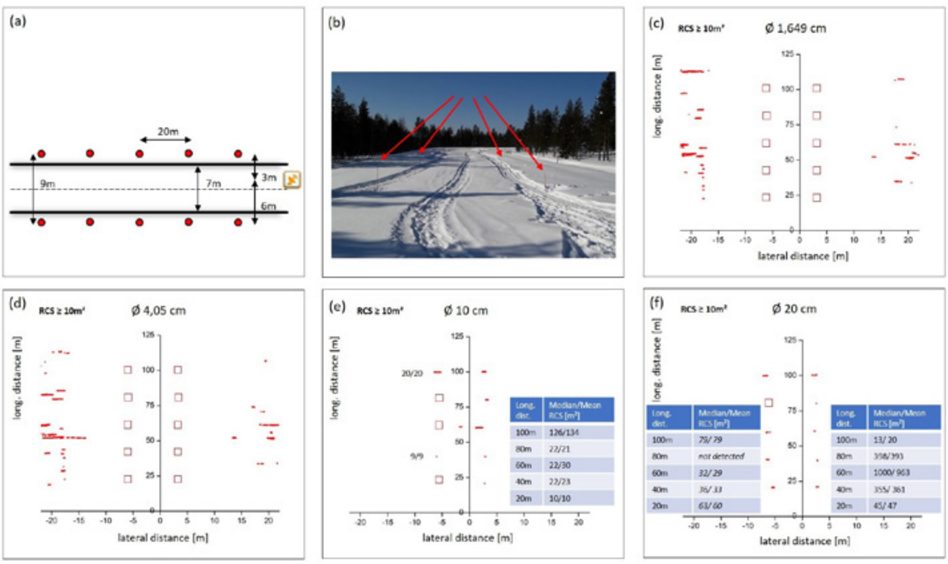

Figure 25 The self-designed reflectors in a road-like case.
(a) Experimental setup in the test field. The longitudinal distance between the reflectors (red dots) is 20 m respectively. The reflectors are positioned 1 m beside the hypothetical road. The radars position is marked in yellow. (b) Photograph of the setup. The red arrows point towards the reflectors on the plastic poles. (c-f) Longitudinal-lateral distance plots for the self-designed reflectors. The red dots show the measured reflections caused by the reflector.

4.4 MOBILE TEST

Based on the results obtained in the last section, a mobile test was prepared. The experimental setup consisted of 10 equal, self-designed reflectors (all Ø 20 cm, five on the left and five on the right side). The distance between the single reflectors was 20 m in a longitudinal direction and 9 m (pairwise) in a lateral direction (see figure 25a and 25b). The reflectors were fixed on top of stationary plastic poles.

Figure 26a and 26b show the experimental conditions before a vehicle drove through the setup. The reflectors appear as isolated points on the left and right side (figure 26a). All ten equally designed reflectors were simultaneously measured in one experiment. The reflector at a longitudinal position of 80 m (left side) was not detectable at the beginning of the measurement but appeared shortly after the vehicle had started to drive. Each reflection in figure 26b represents two reflectors at the same longitudinal position.

While measuring, the sensor from Continental was mounted on the front of the vehicle. The starting position of the vehicle was chosen as shown in figure 25a. 10 s after the data collection had started, the vehicle drove ($v \approx 6{,}5$ km h^{-1}) through the experimental setup. The test field was continuously monitored with the radar while the vehicle drove. Figure 26c-e shows the time evolution of the parameters, lateral- and longitudinal distance, during the measurement. The experimental results show that, not all 10 reflectors are detectable the whole time while the vehicle is driving though the setup. But at least five reflectors were always detectable and ensured an accurate tracking of the prepared test road.

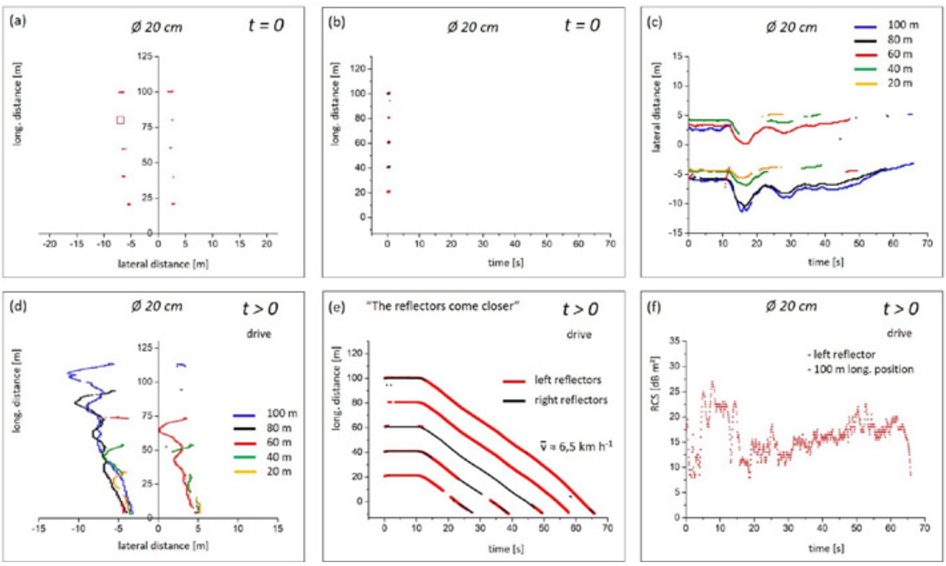

Figure 26 Mobile test with self-designed reflectors in a road-like case.
(a) Longitudinal-lateral distance plot of the setup before the vehicle started to drive. The red dots show the measured reflections caused by the reflector. (b) Longitudinal distance-time plot of the setup before the vehicle started to drive. Each of the five reflections represents two reflectors respectively. (c) Lateral distance-time plot for all 10 reflectors simultaneously. Reflections with the same colour represent reflectors with the same longitudinal distance to the vehicle at t = 0. (d) Longitudinal-lateral distance plot for all 10 reflectors simultaneously while the vehicle

drove through the setup. Reflections with the same colour represent reflectors with the same longitudinal distance to the vehicle at t = 0. (e) Longitudinal distance-time plot for all 10 reflectors simultaneously. The five reflectors on the right side are coloured in black and the reflectors on the left side in red. (f) RCS-time plot for a representative reflector while mobile measurement.

Figure 26f clearly shows a strong angle dependency of the RCS (signal strength) for a representative reflector. The RCS values vary during the 66 s long drive between 10 dBm^2 and 26 dBm^2. The result is in accordance with theoretical expectations introduced in section 2.2.1. The chosen reflector was located in a longitudinal position 100 m away from the starting position of the vehicle (on the left side). The reflector was chosen (out of ten) because it was continuously detectable during the mobile measurement (66 s).

4.5 THE INFLUENCE OF SNOW ON RADAR REFLECTORS

Cold, snowy and icy weather conditions are typical scenarios in Finland and other Nordic countries during the winter period. During this time road markings are hardly visible under the snow which is a challenging task for automated vehicles on the road. Road marker posts such as passive radar reflectors could be the key to overcome detections problems for automated vehicles under extreme weather conditions. Figuring out the influence of snow on the functionality of different types of radar reflectors is the aim of the following tests.

At the beginning, the four reflectors from the maritime sector were positioned 20 m and 80 m (in longitudinal direction) away from the radar, in the test field. Due to the poor results shown in section 4.3.3 the tubular reflector was excluded from the tests. Each reflector was tested in a separate

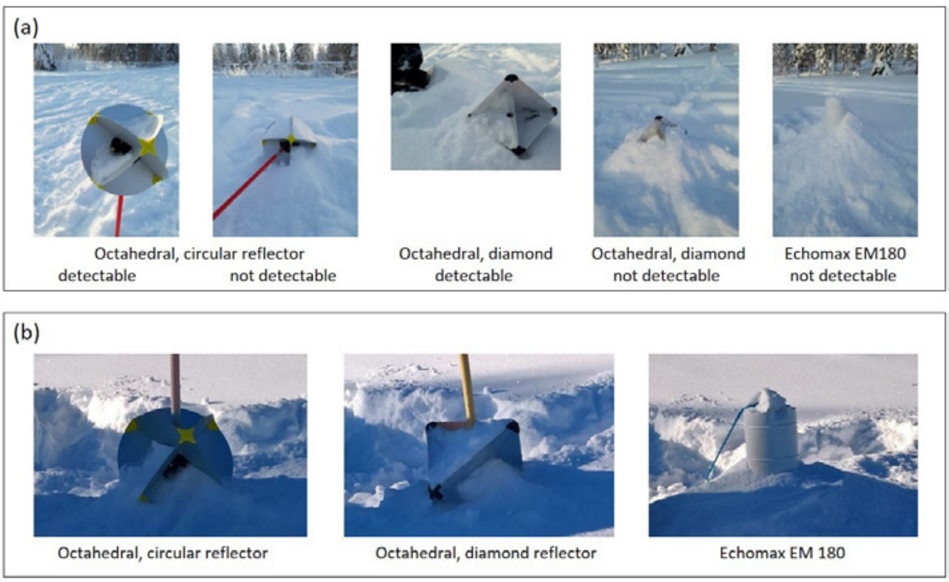

Figure 27 The influence of snow on the functionality of different types of radar reflectors. The longitudinal distance between radar and reflector was 20 m (5 m lateral). (a) Selection of test cases with the radar from Continental. (b) Images show the moment in which the TI radar lost the reflectors as an object.

experiment. After accurate positioning the test field was monitored for 60 s with radars from Continental and TI. The reflectors could be detected as described in section 4.3.1. and 4.3.3. After that, the reflectors were slowly covered by snow in multiple steps and their detectability was constantly monitored.

At both longitudinal distances snow had a very strong influence on the detectability of all tested reflectors. Figure 27a demonstrates a selection of test cases performed with the radar from Continental. Figure 27b shows the moments in which the TI radar lost the reflectors as a detectable object. In contrast, moderate falling snow did not remarkably affect the detectability of the reflectors.

The experiment was repeated with the radar from Furuno (figure 28). It could not clearly be figured out, whether the radar can detect the snow-covered reflectors or not, because the snow pile itself was detectable.

4.6 THE INFLUENCE OF ROADSIDE FURNITURE ON RADAR SIGNALS

In order to study whether typical roadside furniture has a notable effect on future mobile measurements, a lamp pole and poles of different material were illuminated with the radar systems from Continental and TI. The tests should clear-up if the poles are in general detectable with the chosen radars, and if yes, how strong is the detected signal compared to the radar reflectors analyzed in section 4.3.

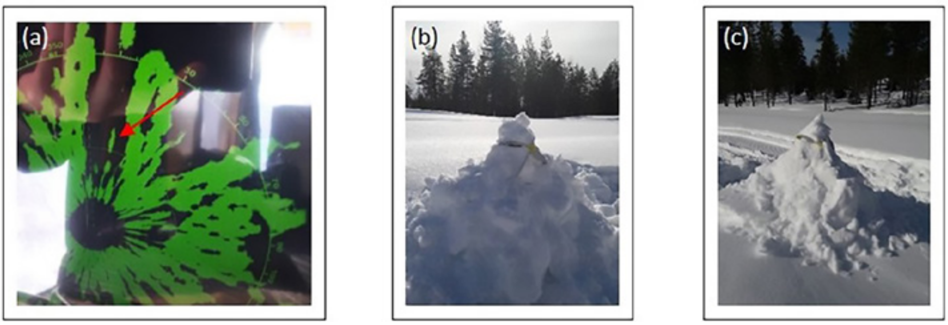

Figure 28 The influence of snow on the functionality of different types of radar reflectors. The longitudinal distance between radar and reflector was 20 m (5 m lateral).
(a) Longitudinal-lateral distance plot measured with the Furuno radar. The red arrow points to the position of the octahedral, circular 40 cm reflector covered with snow. (b) – (c) Snow covered octahedral, circular 40 cm reflector.

4.6.1 Street Lamp Pole

For the tests, the lamp was 7.3 m (in longitudinal direction) away from the radar. The test field was monitored for 10 s with the radar from Continental and 50 s with the radar from TI. The lamp, as a typical representant of roadside furniture, could neither be detected with the radar from Continental (figure 29a), nor with the radar from TI (figure 29c). The chosen noise level was 10 m^2 (Continental) and 8 m^2 (TI). The experiment was repeated with a larger distance (≈30 m) leading to the same result.

As shown in figure 29b, the lamp pole could be detected without noise filtering with the radar from Continental only. The detected signal was very weak ($\sigma = 1.6 \pm 0.1\ m^2$ - in the range of a human, see Figure 6b). The lamp pole could not be detected with the radar from Furuno.

The results indicate that, typical roadside furniture, such as lamp poles, are not practicable as proper radar reflectors for the tested radar systems. The detected signal strength is from one to two magnitudes smaller than some of the tested corner reflectors (e.g. Echomax EM180, σ (80 m) = (126±1) m^2). The big differences in signal strength between lamp poles and corner reflectors makes it easy to distinguish between them.

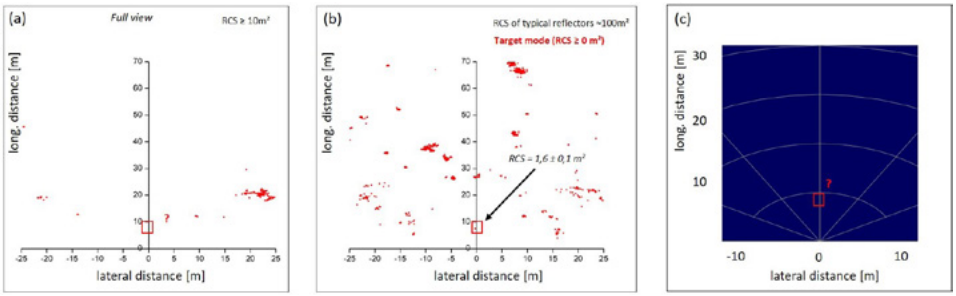

Figure 29 Detectability of roadside furniture. Longitudinal-lateral distance plots with a lamp pole 7.3 m in front of the radar (red boxes).
(a) Continental radar measurement with a noise level of 10 m^2. (b) Continental radar measurement without noise filtering. Shown are all reflections larger than 0 m^2. (c) TI radar measurement with a noise level of 8 m^2.

4.6.2 Poles Composed of Different Material

In the following tests, three circular metal poles composed of different material were tested. Further an angle iron (40 mm x 40 mm x 130 mm) composed of aluminum was measured in different orientations. All tests were performed indoors.

Prior to an experiment, the selected pole was positioned 10 m in longitudinal and 0 m in lateral direction away from the radar. After accurate positioning, the test field was monitored for 25 s with radar from Continental and 10 s with the radar from TI. Each pole was monitored in a separate experiment.

All three of the tested poles were not, or only weakly, detectable with both radars (figure 30a). It can be concluded, that metal pipes are not practicable as proper radar reflectors for the tested radar systems. The detected signal strength is from one to two magnitudes smaller than some of the tested corner reflectors (e.g. Echomax EM180, σ (80 m) = (126±1) m^2). The weak signal strength of the pipes can be explained with their curved surfaces. In contrast to the metal pipes, an angle iron reflects radar waves much better than the circular pipes (figure 30b). The higher error for the rotating angle iron is caused by the angle dependency of backscattered signal strength.

Due to the different diameters of the metal poles, the experiments could not figure out which material reflects best. It can be expected, that copper followed by aluminum reflect radar waves best due to their conductivities [11].

(a)

Marerial	Continental Radar	Texas Instruments Radar
Steal (Ø 28 mm, 1 m length)	not detectable	not detectable
Copper (Ø 64 mm, 1,16 m length)	detectable (weak) (σ = 3.1 ± 1.4 m²)	not detectable
Aluminium (Ø 40 mm, 1.01 m length)	detectable (weak) (σ = 0.56 ± 0.01 m²)	weak detectable

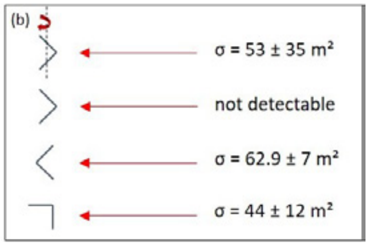

Figure 30 Detectability of metal pipes and angle irons.
(a) Mean RCS values measured for three different metal poles. (b) Mean RCS values measured for an angle iron with different orientations.

5. Summary, Conclusion and Outlook

Autonomous driving could become the most important transformation in the automobile industry in the current century. Accurate and reliable detection of vessels and other objects such as physical land infrastructure is a challenging task for scientists and engineers. Radars and passive radar reflectors could be the key to overcome detection problems under extreme weather conditions, such as falling rain and snow. Radar systems can operate in almost all environmental conditions making them indispensable for technologies supporting autonomous driving, such as advanced emergency braking systems (AEBS) or adaptive cruise control (ACC) [8].

To fully utilize the radar potential for automotive applications under extreme weather conditions, we have conducted a research study that focuses on testing passive roadside radar reflectors. The study contributes to the understanding of prospects and limitations of current technologies and products in the field of autonomous driving with a focus on radars and reflectors.

Section 2 of the report provides basic physical background information concerning radar and reflector techniques. In section 3, three selected radar systems are introduced. The systems from Continental AG, Furuno Electric Co., Ltd. and Texas Instruments Inc. are suitable for transport applications and formed the basis of the measurements described in section 4. Further, four passive radar reflectors in different form and size are described. All of them are used commercially in the maritime sector. In contrast to them, four self-designed corner reflectors are also introduced and discussed.

In order to obtain comparable starting conditions and to characterize typical objects in the surroundings concerning their RSC, a reference measurement was performed with each radar system (section 4.1). In these experiments the test field was only monitored as a background. Equipment or humans were not present on the test track during the measurement. The experiments showed that, the rectangular test field is free from reflections with $\sigma < 16\ m^2$. Based on this result, 16 m^2 was chosen as a threshold for the detectability of targets in further experiments.

In section 4.2 the influence of human presence on the radar signal was studied to estimate its effect on further results. In these experiments a human, dressed in conventional winter clothes, stood and walked in the test field. Additional reflectors were not present on the track during the measurement. The human could not be detected, neither stationary nor walking, with the chosen noise level of $\sigma = 16\ m^2$. It can be concluded that pedestrians will not affect the measurements performed with our setup.

In section 4.3 the experimental results from radar measurements of different radar reflectors are discussed. Four different radar reflectors from the maritime sector were analyzed regarding their reflectivity (RCS) and practicability for our applications. Further, self-designed reflectors of different sizes were tested. In the measurements introduced in section 4.3.1 an octahedral, circular 40 cm reflector was detected with the radar system from Continental on ten longitudinal positions between 10 m and 100 m. The echoes are clearly visible as isolated points and range from σ (80 m) = $(18\pm3)\ m^2$ to σ (60 m) = $(794\pm113)\ m^2$. This deviation is based on the angle dependency of the RCS. The detected accuracy is ±0.1 m in longitudinal and ±0.2 m in lateral direction. The reflector could also be detected with the radars from TI and Furuno. While the echoes, detected with the radar from TI, displayed as isolated points, the echoes measured with the radar from Furuno occurred as diffuse spots in the test field. Further, an experiment in which the reflector was shifted is discussed in section 4.3.2. The results demonstrate that the reflector is almost always detectable, with all three radars, while it is shifted.

These results give a positive prognosis for further tests involving a moving vehicle. In section 4.3.3 three reflectors used in the maritime sector are studied regarding their detectability with different radars. The experiments show that the tubular reflector is not detectable at all with the sensor from Continental. The other two tested reflectors (Echomax EM180 and the octahedral diamond shaped reflector) performed in a similar quality as the octahedral, circular 40 cm reflector. All three tested reflectors were also detectable with the radars from Texas Instruments and Furuno, even the tubular reflector, which was not measurable with the Continental radar. In addition to the commercially used reflectors, four versions of self-designed octahedral corner reflectors are studied in section 4.3.4 and 4.3.5. The RCS values of the Ø20 cm reflector are comparable to those measured for the octahedral, circular 40 cm reflector. Further, they are significantly higher compared to those RCS values detected for the Ø10 cm reflectors. The two smaller (Ø 1.7 cm and Ø 4 cm) self-designed reflectors could not be detected (at any tested positions or angles) with the radar from Continental nor with the radar from Texas instruments. The results indicate, that the self-designed Ø20 cm corner reflectors are a practicable, cheap and easy-to-produce alternative, for our purposes, to current products on the market. On the contrary, the smaller self-designed reflectors are not suitable for the planned applications.

In section 4.4, a mobile test based on the previous results, is discussed. The experimental setup consisted of 10 equal, self-designed reflectors (all Ø 20 cm, five on the left and five on the right side). The distance between the single reflectors was 20 m in a longitudinal direction and 9 m (pairwise) in a lateral direction. All ten equally designed reflectors were simultaneously measured in one experiment. While measuring, the sensor from Continental was mounted on the front of the vehicle. The experimental results show that not all 10 reflectors were detectable the whole time while the vehicle is driving though the setup. But at least five reflectors were always detectable and ensured an accurate tracking of the prepared test road. The measurements show further a strong angle dependency of the RCS for the individual reflectors.

In sections 4.5 and 4.6 the effect of snow and roadside furniture on the radar signal was investigated. It was found, that snow had a very strong influence on the detectability of all tested reflectors independent of the radar system used. In contrast, moderate falling snow did not remarkably affect the detectability of the reflectors. Furthermore, a lamp, as a typical representant of roadside furniture, could neither be detected with the radar from Continental, nor with the radars from TI or Furuno. These results indicate that, typical roadside furniture, such as lamp poles, are not practicable as proper radar reflectors for the tested radar systems.

Finally, it can be stated, that the radar from Continental performed best for our future applications concerning accuracy, resolution, data output and handling. It is further decided to continue working with self-designed Ø20 cm corner reflectors as a practicable, cheap and easy-to-produce alternative to current products on the market. Due to the strong angle dependency of the RCS (signal strength) of a single corner reflector, it is planned to produce a new tubular reflector containing three Ø20 cm corner reflectors. The three reflectors will be rotated against each other and positioned along the same axis in the tube to optimize the visibility. A plastic cover should protect the single reflector plates from falling snow.

Bibliography

[1] Stetter R, Witczak M and Pazera M 2018 Virtual Diagnostic Sensors Design for an Automated Guided Vehicle Applied Sciences 8 702

[2] Teoh E R and Kidd D G 2017 Rage against the machine? Google's self-driving cars versus human drivers Journal of safety research 63 57–60

[3] Yin H and Berger C 2017 - 2017 When to use what data set for your self-driving car algorithm: An overview of publicly available driving datasets 2017 IEEE 20th International Conference on Intelligent Transportation Systems (ITSC) 2017 IEEE 20th International Conference on Intelligent Transportation Systems (ITSC) (Yokohama, 16.10.2017 - 19.10.2017) (IEEE) pp 1–8

[4] Shabbir J and Anwer T 2018 Artificial Intelligence and its Role in Near Future

[5] Rama Rao P V S, Gopi Krishna S, Vara Prasad J, Prasad S N V S, Prasad D S V V D and Niranjan K 2009 Geomagnetic storm effects on GPS based navigation Ann. Geophys. 27 2101–10

[6] Händel C., Konttaniemi H., Autioniemi M. 2018 State-of-the-Art Review on Automotive Radars and Passive Radar Reflectors : Arctic Challenge research project Lapland University of Applied Sciences

[7] Skolnik M I 1983 Introduction to radar systems (International student edition) 2nd edn (Auckland: McGraw-Hill)

[8] Scherr S, Gottel B, Ayhan S, Bhutani A, Pauli M, Winkler W, Scheytt J C and Zwick T 2015 - 2015 Miniaturized 122 GHz ISM band FMCW radar with micrometer accuracy 2015 European Radar Conference (EuRAD) 2015 European Radar Conference (EuRAD) (Paris, France, 09.09.2015 - 11.09.2015) (IEEE) pp 277–80

[9] Avinash Singh Yadav, Sanjiv Kumar 2016 A Review Paper on Radar System International Journal for Innovative Research in Science & Technology 45–7

[10] Christian Wolff Overview of Radar Transmitter http://www.radartutorial.eu/08.transmitters/Radar%20Transmitter.en.html (accessed 16 May 2018)

[11] Demtröder W 2013 Experimentalphysik 6th edn (Berlin, Heidelberg: Springer Spektrum)

[12] Timothy Truckle 2008 Diagram of antenna side lobes. This diagram illustrates how the energy of electro magnetic waves is emitted on an antenna. The line shown in this diagrams usually refers to points where the energy is 3db compared to an iso

emitter. https://en.wikipedia.org/wiki/Radiation_pattern#/media/File:Sidelobes_en.svg (accessed 17 May 2018)
[13] Hofmann H F, Kosako T and Kadoya Y 2007 Design parameters for a nano-optical Yagi–Uda antenna New J. Phys. 9 217
[14] Karthik Ramasubramanian B G 2017 AWR1243 sensor: Highly integrated 76–81-GHz radar front-end for emerging ADAS applications http://www.ti.com/lit/wp/spyy003/spyy003.pdf (accessed 17 May 2018)
[15] Cesar Iovescu S R 2017 The fundamentals of millimeter wave sensors (accessed 17 May 2018)
[16] Larsen T A and Fletcher Henry V. 2013 Low power retroreflective communications system and method US 8,425,09 B2
[17] Lahos E 1996 LIGHTING DEVICE FOR A BICYCLE 5,584,561
[18] Charly Whisky 2016 RCS: Versuch der Darstellung, welcher Anteil der Oberfläche eines kugelförmigen Reflektors bei der Retroreflexion wirksam sein kann. https://commons.wikimedia.org/wiki/File:RCS_reference.jpg (accessed 22 May 2018)
[19] Christian Wolff RCS for Point-Like Targets http://www.radartutorial.eu/01.basics/Radar%20Cross%20Section.en.html (accessed 22 May 2018)
[20] Luneberg technologies 2012 STANDARD RADAR REFLECTORS LIST http://www.radar-reflector.com/wp-content/uploads/2008/07/F7.2_5_TIndex_2012.pdf (accessed 22 May 2018)
[21] Meggitt Target Systems 2015 Luneberg lens: Support products and services http://targetsystems.qinetiq.com/static/media/files/Luneberg_Lens_2015.pdf (accessed 22 May 2018)
[22] Alexey Voronov, Johan Hultén, Johan Wedlin and Cristofer Englund Radar reflecting pavement markers for vehicle automation
[23] Wikimedia Commons 2005 Corner-reflector: Diagram showing working principle of a corner reflector (cat's eye). https://commons.wikimedia.org/wiki/File:Corner-reflector.svg (accessed 23 May 2018)
[24] wdwd 2011 Winkelreflektor3: phasengleiche Reflexion durch gleiche Streckenlängen a+b+c=a'+b'+c' https://commons.wikimedia.org/wiki/File:Winkelreflektor3.svg (accessed 23 May 2018)
[25] Schorschi2 2007 Yachtstellung: Ausrichtung eines Radarreflektors in Yachtstellung https://commons.wikimedia.org/wiki/File:Yachtstellung.jpg (accessed 23 May 2016)
[26] 0x30114 2009 Luneburg lens: Cross-section of the standard Luneburg lens https://commons.wikimedia.org/wiki/File:Luneburg_lens.svg (accessed 23 May 2018)
[27] Armin W. Doerry and Billy C. Brock 2009 Radar Cross Section of Triangular Trihedral Reflector with Extended Bottom Plate: SANDIA REPORT http://prod.sandia.gov/techlib/access-control.cgi/2009/092993.pdf (accessed 23 May 2018)
[28] Osman T I 2014 Analysis of Radar Cross Sectional Area of Corner Reflectors IOSRJEN 04 47–51
[29] Morgan S P 1958 General Solution of the Luneberg Lens Problem Journal of Applied Physics 29 1358–68

[30] Yang B and Friedsam H 2000 Ray-tracing studies for a whole-viewing-angle retroreflector (Illinois, USA)
[31] Google LLC 2018 https://www.google.fi/maps/place/66%C2%B032'52.0%22N+25%C2%B048'36.0%22E/@66.5477778,25.81,439m/data=!3m1!1e3!4m5!3m4!1s0x0:0x0!8m2!3d66.5477778!4d25.81 (accessed 17 May 2018)
[32] Continental AG 2017 ARS 408-21 Premium Long Range Radar Sensor 77 GHz https://www.continental-automotive.com/getattachment/5430d956-1ed7-464b-afa3-cd9cdc98ad63/ARS408-21_datasheet_en_170707_V07.pdf.pdf (accessed 24 May 2018)
[33] Roland Liebske 2016 ARS 404-21 Entry and ARS 408-21 Premium - Short Description: Technical Data http://www.compotrade.ru/i/pdf/ARS404-21_ARS408-21_en_V1.03.pdf (accessed 1 Jun 2018)
[34] Furuno Solid State Doppler Radar: DRS4D-NXT http://www.furuno.com/files/Brochure/334/upload/DRS6ANXT_4DNXT_en_171213.pdf (accessed 31 May 2018)
[35] Furuno The NXT step with doppler Radar technology https://www.furunousa.com/en/products/drs4dnxt (accessed 1 Jun 2018)
[36] Texas Instruments AWR1642: Single-Chip 76-to-81GHz Automotive Radar Sensor Integrating DSP and MCU http://www.ti.com/product/AWR1642 (accessed 31 May 2018)
[37] Texas Instruments AWR1642BOOST AWR1642 Single-Chip 76-to-81GHz Automotive Radar Sensor Integrating DSP and MCU Evaluation Board Image (Angled View) http://www.ti.com/tool/AWR1642BOOST#1 (accessed 31 May 2018)
[38] Krasniqi X and Hajrizi E 2016 Use of IoT Technology to Drive the Automotive Industry from Connected to Full Autonomous Vehicles IFAC-PapersOnLine 49 269–74
[39] Condon, Edward J and Kolbe, Edward and others (ed) 1978 Radar reflectors for boats (Marine electronics A28 no. 41)
[40] Texas Instruments AWR1642 single chip sensor and its range, field of view capability https://e2e.ti.com/blogs_/b/behind_the_wheel/archive/2017/05/16/giving-cars-advanced-vision-through-ti-mmwave-sensors (accessed 31 May 2018)
[41] Luke S 2007 Performance investigation of marine radar reflectors on the market.

This report demonstrates and discusses results of passive roadside radar reflector practical tests carried out in Rovaniemi during winter period 2017-2018. The selection of the passive radar reflectors for actual automotive radar tests on the Aurora intelligent test road in Muonio has been made based on this report.

This report has been developed in the Arctic Challenge research project. The Arctic Challenge research project is funded by the Finnish Transport Agency (FTA) and the Finnish Transport Safety Agency (TraFi). The project is part of the Aurora intelligent road project of the Finnish Transport Agency and the NordicWay2 project funded by the Connecting Europe Facility of the European Union. The testing weeks for the research project will take place on the 10-km-long test stretch of the Aurora Vt21 (E8) intelligent road section in the years 2017–2019. Furthermore, the project is part of the Traffic Lab cooperation. The contracting partners involved in the research project include Dynniq Finland Oy, Indagon Oy, Infotripla Oy, Lapland University of Applied Sciences Oy, Roadscanners Oy, Sensible 4 Oy and VTT Technical Research Centre of Finland Oy.

Co-financed by the European Union
Connecting Europe Facility

LAPIN AMK
Lapland University of Applied Sciences

ROADSCANNERS

VÄYLÄ
Finnish Transport Infrastructure Agency

aurora
snowbox.fi

TRAFICOM

LAPIN AMK
Lapland University of Applied Sciences

www.lapinamk.fi

ISBN 978-952-316-279-2